Chemical and Vibrational Relaxation of an Inviscid Hypersonic Flow

ALBERT D. WOOD,* JAMES F. SPRINGFIELD,† AND ADRIAN J. PALLONE‡
Avco Corporation, Wilmington, Mass.

The conservation equations for an inviscid, nonconducting fluid with chemical and vibrational relaxation are put into characteristic form for the determination of hypersonic flow fields. Application of the analysis to the simpler case of vibrational equilibrium is also discussed. An approximation is presented wherein the nonequilibrium terms are considered along the streamline characteristics but are neglected along the Mach line. Results at typical entry conditions in the earth's atmosphere are determined for pointed bodies with and without vibrational equilibrium and for blunted bodies with vibrational equilibrium. The validity of this approximation is demonstrated by comparison with results of the corresponding exact calculation (i.e., with the nonequilibrium terms included in the Mach line relationships) for the blunt body in vibrational equilibrium. Comparisons are also made with results from frozen and equilibrium analyses. The effects of both chemical and vibrational relaxation, and variation of nose bluntness, on the downstream composition of the gas are shown to be appreciable. A comparison with results of a simpler one-dimensional, nonequilibrium streamtube analysis indicates that the latter is adequate in many cases.

Nomenclature

a = locally frozen speed of sound
c = velocity
e = internal energy of mixture per unit mass
e_{vj} = vibrational energy per unit mass of a vibrationally relaxing species j
F = function defined by Eq. (13)
H = stagnation enthalpy of mixture per unit mass
k = 1 or 2 for a right- or left-running characteristic, respectively
K_D, K_R = dissociation and recombination rate constants, respectively
K_1, K_2 = forward and reverse rate constants, respectively
m = number of vibrationally relaxing species
m_0 = molecular weight of undissociated mixture
m_i = molecular weight of species i
M = Mach number based on locally frozen sound speed
n = number of species of mixture
Ne = electron concentration, electrons/cm^3
N_j = total number of vibrational states of species j
p = pressure
R = universal gas constant
R_j = R/m_j
R_0 = R/m_0
s = entropy of mixture per unit mass
s_i = entropy per unit mass of species i at reference pressure p_0 [see Eq. (21)]
T = translational temperature
T_{vj} = vibrational temperature of species j
u_∞ = freestream velocity
V_j = vibration-dissociation coupling function of species j, as defined by Eq. (19)
x, r = coordinates of a cylindrical coordinate system
X_i = concentration of species i, moles/mole of undissociated mixture
α_k = distance measured along a Mach line characteristic
γ = ratio of specific heats
Γ_i = total rate of production of species i by all reactions, moles/mole of undissociated mixture per unit time
ϵ = 0 or 1 for two-dimensional or axisymmetric flows, respectively
θ = inclination of velocity with respect to the horizontal
Θ_j = characteristic temperature of molecular vibration for species j
μ_i = chemical potential per unit mass of species i
ξ, η = coordinates of streamline coordinate system (ξ measured along streamline, η normal to streamline)
ρ = density of mixture
τ_j = vibrational relaxation time of species j

Subscripts

i = species i of mixture
j = vibrationally relaxing species j of mixture
∞ = freestream conditions

Presented as Preprint 63-441 at the AIAA Conference on Physics of Entry into Planetary Atmospheres, Cambridge, Mass., August 26–28, 1963; revision received June 23, 1964. The research was supported by the Ballistic Systems Division, Air Force Systems Command, U. S. Air Force, under Contract No. AF04(694)-239. The authors wish to express their appreciation to J. Derek Teare of the Avco Everett Research Laboratory for making available his nonequilibrium streamtube technique, which formed a partial basis for this investigation. The work of Anthony A. Pappas of Avco's Research and Advanced Development Division, who carried out the programing of the analysis for use on an IBM 7094 digital computing machine, is also gratefully acknowledged.

* Chief, Gasdynamics Research Section, Research and Advanced Development Division. Member AIAA.
† Senior Scientist, Gasdynamics Research Section, Research and Advanced Development Division.
‡ Manager, Aerophysics Department, Research and Advanced Development Division.

I. Introduction

ONE of the most important aspects of hypersonic flight calculations involves the correct determination of the complete flow field about a given body. Of particular interest in such a computation is the determination of the inviscid flow field, both for a knowledge of the flow itself, as well as for the establishment of the boundary conditions necessary for associated wake and boundary-layer studies. Several techniques exist for an exact determination of such flow fields, provided the gas has an equilibrium or frozen composition. In particular, for the subsonic region, which exists in the vicinity of a blunted nose, both direct and inverse methods are available.[1, 2] For the supersonic region, the analysis is carried out by application of the method of characteristics.[3] Such techniques are all well known and will not be further discussed here.

However, these relatively simple methods are not sufficient to describe accurately re-entry flight at extreme altitudes where the high velocities and low atmospheric densities encountered may give rise to significant relaxation effects, both with regard to chemistry and vibrational energy level.

In the past, such effects have been crudely considered by application of the thermochemical rate and vibrational relaxation expressions along streamlines determined from an equilibrium or frozen analysis, assuming the pressure distribution along these streamlines is preserved.[4, 5] The availability of more sophisticated techniques in which the chemical and vibrational relaxation are coupled with the fluid dynamics is somewhat limited. Some work has been done for chemical relaxation in the subsonic region about the nose of a blunted body,[6, 7] and recently the effects of vibrational relaxation have been added.[8] Several analyses for slender wedges and cones are also available.[9–12] These latter analyses, however, involve many simplifying assumptions made possible by the relative smallness of the nonequilibrium effects. Moreover, Ref. 9 is restricted to chemical relaxation alone, and Refs. 10–12 consider only vibrational relaxation. A more general finite-difference technique has been formulated,[13] but it assumes vibrational equilibrium and has only been applied to nozzle flows. Finally, two exact characteristics formulations for chemical nonequilibrium,[14, 15] as well as a general treatment involving both chemical and internal relaxation,[16] have been developed; however, to the authors' knowledge, there are presently no calculations available from these analyses.

In the following sections, both exact and approximate nonequilibrium characteristics techniques are summarized for external flows with and without the assumption of vibrational equilibrium. Selected results of the approximate analysis are presented for a blunted body under the restriction of vibrational equilibrium and compared with similar results obtained from both an exact analysis and the corresponding equilibrium and frozen calculations. Finally, the effects of vibrational relaxation are illustrated in calculations carried out for an ogival body, using the approximate technique. Additional results, together with more details on the derivation, may be found in Ref. 17.

II. Basic Equations

The analysis will be restricted to the steady, two-dimensional or axisymmetric flow of an inviscid, nonconducting gas. The gas will be considered as a chemically and vibrationally relaxing mixture of monatomic and diatomic ideal gases. Local thermodynamic equilibrium within classes of degrees of freedom will be assumed, with the result that a Boltzmann distribution exists for each class, thereby permitting the definition of a temperature, entropy, and energy for each class. It will be assumed that the translational and rotational degrees of freedom are in equilibrium. The attainment of equilibrium between these and the vibrational degrees of freedom of the diatomic molecules is governed by the appropriate rate processes in a manner similar to the chemical relaxation of the individual species of the mixture.

Thus, in addition to the usual pair of independent thermodynamic variables, such as temperature and pressure, needed to specify an equilibrium or frozen flow, the state of the relaxing system considered here requires the specification of the species concentrations X_i for each of the n species of the mixture and the vibrational energies e_{v_j} for each of the m vibrationally relaxing species of the mixture. The determination of these quantities requires simultaneous solution of the usual equations of conservation of mass, momentum, and energy, together with the species production and vibrational relaxation rate equations and the appropriate equations of state.

A streamline coordinate system is introduced wherein ξ and η denote distance measured along and normal to the streamlines, respectively, and θ is the inclination of the velocity c with respect to the horizontal. Then, if ρ is density, p is pressure, and e is the internal energy of the mixture per unit mass, the conservation equations are given as

$$\frac{\partial c}{\partial \xi} + \frac{c}{\rho}\frac{\partial \rho}{\partial \xi} + \frac{c\epsilon}{r}\sin\theta + c\frac{\partial \theta}{\partial \eta} = 0 \tag{1}$$

$$c\frac{\partial c}{\partial \xi} = -\frac{1}{\rho}\frac{\partial p}{\partial \xi} \tag{2}$$

$$c^2\frac{\partial \theta}{\partial \xi} = -\frac{1}{\rho}\frac{\partial p}{\partial \eta} \tag{3}$$

$$e + \frac{p}{\rho} + \frac{c^2}{2} = H \tag{4}$$

In Eq. (1), ϵ is 0 or 1 for two-dimensional or axisymmetric flows, respectively, and r is the radial coordinate of an axisymmetric flow. The stagnation enthalpy per unit mass is H, a constant throughout the flow field.

The rate equations for species production have the form

$$c\frac{\partial X_i}{\partial \xi} = \Gamma_i(\rho, T, X_1, \ldots, X_n, e_{v_1}, \ldots, e_{v_m}) \qquad i = 1, 2, \ldots, n \tag{5}$$

where T is the translational temperature. The quantities Γ_i represent the total production of species i per unit time by all the reactions. They are known functions of the indicated variables, based on the known species partition functions and experimentally determined reaction rate expressions and relaxation times. The presence of the vibrational energy terms represents the coupling of the vibrational relaxation with the dissociation.

The corresponding rate equations for vibrational relaxation are given in the usual linear form

$$c\frac{\partial e_{v_j}}{\partial \xi} = \frac{e_{v_j}(T) - e_{v_j}}{\tau_j} \qquad j = 1, 2, \ldots, m \tag{6}$$

with $e_{v_j}(T)$ being the vibrational energy that would exist if the vibrational degrees of freedom were in equilibrium with the translational temperature. The quantity τ_j is the experimentally determined vibrational relaxation time and is, in general, a function of pressure and translational temperature. The e_{v_j} are defined in terms of the corresponding vibrational temperatures T_{v_j} by the usual simple harmonic oscillator model

$$e_{v_j} = \frac{R_j\Theta_j}{\exp(\Theta_j/T_{v_j}) - 1} \tag{7}$$

where R_j is the universal gas constant divided by the molecular weight of species j, and Θ_j is the characteristic temperature of molecular vibration.

The system is completed by introduction of the thermal and caloric equations of state. The thermal equation is

$$p = \rho R_0 T \sum_{i=1}^{n} X_i \tag{8}$$

where R_0 is the universal gas constant divided by the molecular weight of the undissociated mixture.

Inasmuch as the vibrational energies of those species undergoing vibrational relaxation are independent variables of the problem, the caloric equation of state is written in functional form as

$$e = e(T, X_1, \ldots, X_n, e_{v_1}, \ldots, e_{v_m}) \tag{9}$$

By virtue of the assumption that the components of the mixture are ideal gases, the precise form of this relation is known.[17]

Equations (1–6, 8, and 9) represent a set of $6 + n + m$ relations in the $6 + n + m$ unknowns c, θ, p, ρ, T, e, $X_1, \ldots, X_n$, $e_{v1} \ldots, e_{v_m}$ and, hence, completely determine the flow

field. In order to put them in characteristics form, an alternative to the thermal equation of state (8) is introduced. In functional form, it is[16]

$$p = p(\rho, s, X_1, \ldots, X_n, e_{v_1}, \ldots, e_{v_m}) \tag{10}$$

where s denotes the entropy (per unit mass) of the mixture. A locally frozen speed of sound may then be defined as[16]

$$a^2 = \left(\frac{\partial p}{\partial \rho}\right)_{s, X_1, \ldots, X_n, e_{v_1} \ldots, e_{v_m}} \tag{11}$$

together with the associated Mach number $M = c/a$. The significance of this sound speed will be discussed later.

Making use of Eqs. (10) and (11), the variation of pressure along a streamline may be written as

$$\frac{\partial p}{\partial \xi} = a^2 \frac{\partial \rho}{\partial \xi} + F \tag{12}$$

The function F represents the pressure variation due to chemical and vibrational relaxation. It has the form

$$F = \left(\frac{\partial p}{\partial s}\right)\left(\frac{\partial s}{\partial \xi}\right) + \sum_{i=1}^{n}\left(\frac{\partial p}{\partial X_i}\right)\left(\frac{\partial X_i}{\partial \xi}\right) + \sum_{j=1}^{m}\left(\frac{\partial p}{\partial e_{v_j}}\right)\left(\frac{\partial e_{v_j}}{\partial \xi}\right) \tag{13}$$

where it is understood that the partial differentiation of the pressure is carried out with the remaining variables in Eq. (10) held constant. It should be noted that, for equilibrium or frozen flows, the state of the gas is completely determined by specification of two independent thermodynamic variables. For these cases, the thermal equation of state (10) may be simplified to express p as a function of ρ and s alone, and the locally frozen sound speed, as defined in Eq. (11) and used in Eq. (12), is replaced by the appropriate equilibrium or perfect gas relation (i.e., the partial derivative of pressure with respect to density, holding entropy alone constant). Then, since there is also no entropy variation along a streamline for such flows, the function F will be absent from Eq. (12) and, hence, from both equilibrium and frozen analyses.

Introducing Eq. (12) into the system of partial differential equations (1–3), it may be shown that they reduce to a pair of ordinary differential equations

$$\frac{(M^2 - 1)^{1/2}}{\rho c^2} dp + (-1)^k d\theta = \frac{d\alpha_k}{M}\left(-\frac{\epsilon \sin\theta}{r} + \frac{F}{\rho a^2}\right) \tag{14}$$

when written along the right- and left-running Mach lines defined by the relations

$$d\eta/d\xi = (-1)^k (M^2 - 1)^{-1/2} \tag{15}$$

Thus the Mach lines are characteristics of the flow along which the distance $d\alpha_k$ is measured, with $k = 1, 2$ for right- or left-running characteristics, respectively. The speed of sound a and the function F are defined by Eqs. (11) and (13) and presented in more specific form, suitable for numerical calculations, in Ref. 17.

Similarly, if the partial differential equations (5) and (6) are written along a streamline, they reduce to the ordinary differential equations

$$dX_i = (\Gamma_i/c) d\xi \qquad i = 1, 2, \ldots, n \tag{16}$$

$$de_{v_j} = \frac{e_{v_j}(T) - e_{v_j}}{c\tau_j} d\xi \qquad j = 1, 2, \ldots, m \tag{17}$$

and hence the streamlines are also characteristics of the flow.

One more relation may be found from Eq. (4), differentiated along a streamline. Introducing Eqs. (2, 8, 9, 16, and 17), the final result has the form

$$dT = f_1(\rho, T, X_1, \ldots, X_n) dp + f_2(\rho, T, c, X_1, \ldots, X_n, e_{v_1}, \ldots, e_{v_m}) d\xi \tag{18}$$

which is also an ordinary differential relation. The precise form of the coefficient functions f_1 and f_2 may be found in Ref. 17.

Thus it is seen that the Mach lines and streamlines form a system of characteristics along which Eqs. (14 and 16–18) may be solved for p, θ, T, $X_1, \ldots, X_n$, $e_{v_1}, \ldots, e_{v_m}$, thereby completely determining the state of the gas. The remaining variables ρ, e, and c may then be found from Eqs. (8, 9, and 4), respectively.

At this point it seems appropriate to make some remarks concerning the nature of the speed of sound for a nonequilibrium flow about which there is some ambiguity.[14] Inasmuch as the wave front propagates into a medium that has no way of knowing about approaching disturbances, it travels at the locally frozen sound speed, whereas the remainder of the signal will follow at some different speed. The sound speed that arises in the derivation of the nonequilibrium characteristics relations is also the locally frozen value, and hence the direction of the associated Mach line characteristics is determined from this speed. For increasing chemical and vibrational relaxation rates, this phenomenon will require a reduction in mesh size in order to achieve a given degree of accuracy. Indeed, the problem is of a singular perturbation nature, inasmuch as the Mach line characteristics (and hence wave front propagation speed) change discontinuously as equilibrium is approached. The phenomenon is discussed in more detail in Refs. 14 and 16.

III. Relaxation Phenomena

Restricting attention to problems of entry into the earth's atmosphere, the seven predominant species involved in the chemical relaxation represented by Eqs. (16) are O_2, N_2, O, N, NO, NO^+, and electrons. The reactions thought to be the most important in this relaxation process are summarized as reactions 1–7 of Table 1. The indicated rate constants have been taken from Ref. 4. Although more recent tabulations are available,[18, 19] the differences associated with the use of these tabulations will not alter the general nonequilibrium trends.

The first six reactions are coupled directly to the fluid dynamical equations, as indicated in the previous section. The electronic reaction 7, however, is not coupled to the remainder of the flow-field calculations; rather, it is considered only after the nonequilibrium composition of the gas has been determined with this reaction neglected.

It should be noted that the electronic reaction considered here will be the primary source of electrons, provided the flow-field temperature is not too high. At extreme temperatures, however, additional ionization reactions will become significant. A discussion of this behavior may be found, for example, in Ref. 20.

In addition to the rates of Table 1, the reverse rates are also needed. For vibrational equilibrium, the ratio of forward to reverse rates is the equilibrium constant, which may be determined from the individual species partition functions. The values of these constants, as used in this analysis, are essentially equivalent to the simplified expressions of Ref. 18.

For a vibrationally relaxing species, the vibrational nonequilibrium must be coupled with the dissociation process. Unfortunately, at the present time the precise nature of this coupling is not firmly understood. In fact, a perusal of the literature indicates that several alternative schemes have been proposed (see, for example, Refs. 21–25). In view of this uncertainty, the relatively simple model of Ref. 21 will be used here.

Specifically, this model assumes that the rate constants for all the vibrational levels of a given species are equal in the equations of vibrational excitation. Throughout the relaxation process the fraction of molecules of a particular species at a given vibrational level is assumed to satisfy a Boltzmann distribution about the local vibrational tempera-

ture of that species. Under these assumptions, it may be shown that the dissociation rate for a vibrationally relaxing species is the product of the vibrational equilibrium rate and a vibration-dissociation coupling function V_i given as

$$V_i = \frac{1}{N_i}\left[\frac{1 - \exp\{-N_i\Theta_i[(1/T_{v_i}) - (1/T)]\}}{1 - \exp\{-\Theta_i[(1/T_{v_i}) - (1/T)]\}}\right] \times \frac{1 - \exp(-\Theta_i/T_{v_i})}{1 - \exp(-\Theta_i/T)} \quad (19)$$

where N_i is the total number of vibrational states. This coupling function is used only so long as the vibrational temperatures are less than the translational temperature. After a vibrational temperature becomes equal to the translational temperature, the particular species is assumed to stay in vibrational equilibrium, with the coupling function set equal to unity, and the appropriate vibrational relaxation equation (17) eliminated. The vibrational energy of this species then is no longer an independent state variable.

For this investigation, vibrational relaxation of O_2 and N_2 has been considered, together with its effect on the dissociation reactions 1 and 2 of Table 1. The appropriate equations of vibrational excitation, together with the vibrational relaxation times, are given as reactions 8 and 9 in Table 1. The notation $O_2^{(v)}$ and $N_2^{(v)}$ is used to denote vibrationally excited molecules.

It should be emphasized that the use of this simplified model represents only an approximation to the actual mechanism. A fairly comprehensive review of other more exact models is presented in Ref. 22. One area in which the simplified model is open to question is in regard to the assumption of equal rate constants for dissociation from all vibrational levels, which is discussed in Refs. 23 and 24. Also, although the simplified model accounts for the effects of vibrational nonequilibrium on the dissociation rates (i.e., the so-called CVD method), the simultaneous influence of the dissociation on the vibrational relaxation (CVDV) has been neglected. A discussion of this is given in Ref. 25. Nevertheless, in spite of these approximations, the simplified

Table 1 Rate constants and vibrational relaxation times[a]

No.	Reaction	Catalyst M	Rate Constant or Vib. Relaxation Time
1.	$O_2 + M + 5.1\,ev \underset{K_R}{\overset{K_D}{\rightleftharpoons}} O + O + M$	O_2	$K_D = 1.2 \times 10^{23}\, T^{-2} \exp(-59373/T)$
		O	$K_D = 3.2 \times 10^{23}\, T^{-2} \exp(-59373/T)$
		N, N_2, NO	$K_D = 3.6 \times 10^{18}\, T^{-1} \exp(-59373/T)$
2.	$N_2 + M + 9.8\,ev \underset{K_R}{\overset{K_D}{\rightleftharpoons}} N + N + M$	N	$K_R = 7.6 \times 10^{20}\, T^{-3/2}$
		N_2	$K_R = 1.5 \times 10^{20}\, T^{-3/2}$
		O, O_2, NO	$K_R = 5.0 \times 10^{19}\, T^{-3/2}$
3.	$NO + M + 6.5\,ev \underset{K_R}{\overset{K_D}{\rightleftharpoons}} N + O + M$	O, O_2, N, N_2, NO	$K_R = 8.7 \times 10^{20}\, T^{-3/2}$
4.	$NO + O + 1.4\,ev \underset{K_2}{\overset{K_1}{\rightleftharpoons}} O_2 + N$	———	$K_2 = 1.0 \times 10^{12}\, T^{1/2} \exp(-3120/T)$
5.	$N_2 + O + 3.3\,ev \underset{K_2}{\overset{K_1}{\rightleftharpoons}} NO + N$	———	$K_2 = 1.3 \times 10^{13}$
6.	$N_2 + O_2 + 1.9\,ev \underset{K_2}{\overset{K_1}{\rightleftharpoons}} NO + NO$	———	$K_2 = 2.4 \times 10^{23}\, T^{-5/2} \exp(-43000/T)$
7.	$N + O + 2.8\,ev \underset{K_2}{\overset{K_1}{\rightleftharpoons}} NO^+ + e^-$	———	$K_2 = 1.8 \times 10^{21}\, T^{-3/2}$
8.	$O_2 + M + \Delta H \rightleftharpoons O_2^{(v)} + M$	O_2	$\tau = \dfrac{2.0 \times 10^{-10}\, T^{5/6} \exp(218.3\, T^{-1/3})}{p\,[1 - \exp(-2228/T)]}$
		O, N, N_2, NO	$\tau = \dfrac{1.0 \times 10^{-9}\, T^{5/6} \exp(218.3\, T^{-1/3})}{p\,[1 - \exp(-2228/T)]}$
9.	$N_2 + M + \Delta H \rightleftharpoons N_2^{(v)} + M$	O_2, N_2, O, N, NO	$\tau = \dfrac{6.4 \times 10^{-7}\, T^{1/2} \exp(192\, T^{-1/3})}{p\,[1 - \exp(-3336.6/T)]}$

[a] T in °K, concentrations in moles/cm^3, time and τ in seconds, and p in dynes/cm^2.

vibrational model used here can be expected to yield qualitatively correct results with regard to the effects of combined chemical and vibrational relaxation on the flow field.

More detail on both the chemical and vibrational relaxation models as used in this analysis may be obtained from Refs. 18 and 26.

IV. Numerical Procedure

In view of the complexity of the function F, an approximation is suggested whereby it is neglected in the Mach line characteristics relations (14), thus reducing them to frozen (or equilibrium) form. Basically, such a simplification results in the local combination of a perfect gas characteristics technique with a nonequilibrium streamtube analysis (such as that of Ref. 4) to give a useful nonequilibrium characteristics approximation.

The use of such an approximation is suggested by the observation that for a large class of bodies the pressure distribution within the hypersonic flow field does not significantly vary between the two extremes of equilibrium and frozen flow. Inasmuch as the Mach line characteristics relations are used only to determine the pressure and geometry, the neglect of the nonequilibrium terms in these relations would not be expected to produce serious discrepancies. Moreover, the effect of the approximation is minimized by use of the correct local values of all other properties as determined from the nonequilibrium streamline characteristic relations. This in turn will influence the pressure and geometry through the averaging of properties along the Mach line characteristics for use in successive iterations of the Mach line relations.

The technique whereby the calculation is carried out is illustrated in Fig. 1, where the characteristics grid for an interior point is shown. Using properties at A and B, together with the Mach line relations (14) and (15), the coordinates, flow angle and pressure are approximated at C. Point P is determined by averaging the flow angle between P and C and assuming it to vary linearly from A to B. The remaining properties at P are calculated by assuming a similar linear variation between A and B. Temperature, species concentrations, and nonequilibrium vibrational energies at C are then found by application of a Runge-Kutta numerical integration technique to the nonequilibrium streamline relations (16–18), assuming a linear pressure distribution from P to C. Remaining properties that may be desired are found from the appropriate equations of state. The procedure is iterated until any desired degree of accuracy is achieved.

A similar method is used for the less general case of complete vibrational equilibrium, except that the vibrational relaxation equations (17) are neglected everywhere, the vibration-dissociation coupling functions are set equal to unity, and all vibrational temperatures are set equal to the translational temperature. The vibrational energies e_{vi} no longer occur as independent state variables.

Corresponding procedures are followed for body and shock points, except that one of the Mach line relations is replaced by either the known body slope (for a body point) or the Rankine-Hugoniot relations (for a shock point). In this latter case, the freestream species concentrations are preserved across the shock. Freestream vibrational energies are also maintained unless vibrational equilibrium is assumed, in which case the vibrational energies are based on the translational temperature behind the shock.

A true evaluation of the approximate technique described here can only be had by comparing the results with those obtained from an exact analysis, where the function F is included in the Mach line relationships. Such a comparison will be made under the assumption of vibrational equilibrium, rather than for the more complex case of simultaneous

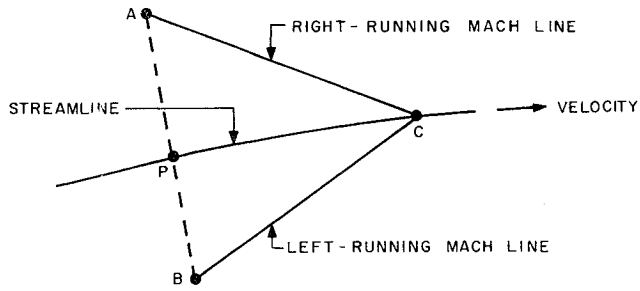

Fig. 1 Geometry of characteristics grid.

chemical and vibrational relaxation. The function F may then be shown[17] to reduce to the somewhat simpler form

$$F = -\frac{1}{Tc}\left(\frac{\partial p}{\partial s}\right)\sum_{i=1}^{n}\frac{m_i}{m_0}\mu_i\Gamma_i + \frac{1}{c}\sum_{i=1}^{n}\left(\frac{\partial p}{\partial X_i}\right)\Gamma_i \quad (20)$$

where m_0 and m_i denote the molecular weights of the undissociated mixture and species i, respectively, and μ_i is the chemical potential per unit mass of species i. Again it is understood that the partial differentiation of the pressure is carried out with the remaining variables in Eq. (10) (exclusive of the e_{vi}, which are absent for vibrational equilibrium) held constant. These pressure derivatives are evaluated numerically from the relation determining entropy as a function of pressure, density, and species concentrations. Following Ref. 27, this relation is taken to be the same as the corresponding equilibrium relation

$$\frac{s}{R_0} = \sum_{i=1}^{n} X_i\left[\frac{s_i}{R_i} - \ln\left(X_i\Big/\sum_{i=1}^{n}X_i\right) - \ln\frac{p}{p_0}\right] \quad (21)$$

where s_i is the entropy per unit mass of species i at pressure p_0. It is a known thermodynamic function of temperature T or, introducing the thermal equation of state (8), of pressure, density, and species concentrations.

The computational technique, whereby the exact calculation is carried out, is essentially the same as for the approximate method, the only difference being the inclusion of the function F in the Mach line characteristics relationships and its consequent evaluation at each characteristics grid point.

Some of the numerical problems that have been encountered in this analysis are worthy of mention. It will be noted that the Mach line characteristics formulation used here [Eq. (14)] is one in which pressure and flow angle are the dependent variables. An alternative system, wherein velocity and flow angle are used, has been avoided because of the resulting introduction of the additional variable entropy into the relations. Similarly, the streamline characteristic relation (18) has been formulated for temperature rather than the more customary quantity entropy.[14] Both of these choices have been made specifically to reduce the large errors observed to arise by the authors and others[11] if entropy is used.

As with any characteristics technique applied to the flow past a blunted body, the subsonic-transonic portion of the flow in the vicinity of the nose must first be determined by other means. Although the accuracy of this calculation will, of course, influence the downstream characteristics solution, the effect has not been found to be critical. Small errors or inconsistencies are generally overcome by the relatively strong relaxation phenomena taking place in the characteristics calculations near the sonic line. The problem is even less critical for pointed bodies, since the solution near the nose may be determined with great accuracy from an appropriate conical flow analysis.

An additional numerical difficulty is encountered for the exact characteristics analysis in the evaluation of the pres-

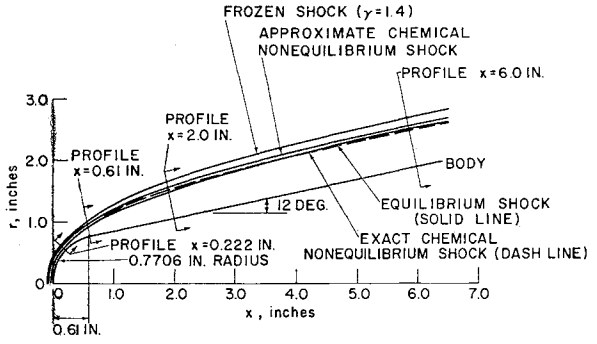

Fig. 2 Geometry for blunted body.

sure derivatives $(\partial p/\partial X_i)$ of Eq. (20) immediately behind the bow shock where only the freestream species are present. In this case differentiation of the mixing term $X_i \ln X_i$ in Eq. (21) will result in a logarithmic singularity for each of the missing species. The situation is physically unreal and may be resolved by specifying a proper limiting form of the Mach line characteristic relation at the shock. A simpler numerical alternative, which has been used here, is to specify arbitrary small amounts of the missing species in the freestream. (In this case, concentrations of the order of 10^{-6} have been introduced for the species O, N, and NO.) Clearly, such a procedure should not significantly affect the results. Moreover, this procedure is physically sound since, as is known from thermodynamic considerations, traces of these species will be present.

Aside from these particular difficulties, the only other problems that might be expected to be encountered would be related to the chemical and vibrational relaxation mechanism itself. As a result of the availability of the established and thoroughly tested nonequilibrium streamtube technique of Ref. 4, however, no such difficulties have been experienced here.

The actual computations have been carried out on an IBM 7094 computer. The time required for the calculation of a single grid point will vary widely, depending on the grid size and the rate of the relaxation processes. Some idea of typical running times may be obtained, however, from a consideration of the calculations required for the 6-in.-long blunted body of Fig. 2. Twelve grid points were specified along the initial line at $x = 0.222$ in. in order to assure a sufficiently fine spatial resolution of the flow field. The resulting running time for the nonequilibrium characteristics portion of the flow field (i.e., downstream of the initial line) was of the order of 90 min for both approximate and exact analyses, with about 60 min being required for the first 2.5 in. The longer running time used for the forebody calculation is due to the more rapid relaxation in this region and to the resulting greater number of required Runge-Kutta integration steps.

In contrast to the nonequilibrium calculation, the corresponding equilibrium of frozen solutions were determined in about 8 min. The difference, which is due solely to the inclusion of the relaxation processes along the streamline characteristics, serves to indicate the extreme complexity of these processes.

V. Results

The effects of chemical relaxation on the flow past a blunted body have been determined for the sphere-cone configuration of Fig. 2 under the assumption of vibrational equilibrium. Specifically, the body is a 12° half-angle spherically blunted cone with a nose radius of 0.7706 in. traveling in air at the typical entry conditions of 23,000-fps velocity and 200,000-ft alt.

Results have been determined for both the exact and approximate characteristics techniques. They are compared with similar results obtained for equilibrium and frozen (specific heat ratio of 1.4) flows, also calculated by the method of characteristics. In all cases, the characteristics solution has been started at the body normal that intersects the body at $x = 0.222$ in., just beyond the sonic point. Properties along this normal have been found by first determining the subsonic flow field about the nose of the vehicle. A direct technique has been used in this calculation, with the method of Ref. 1 being applied for the equilibrium and frozen flows and that of Ref. 8 (the nonequilibrium analog to Ref. 1) for the nonequilibrium flows.

The resulting shock geometry is presented in Fig. 2. The exact and approximate nonequilibrium shocks coincide initially, as they are both based on the same blunt-body solution. Downstream, however, they diverge somewhat, indicating the discrepancy resulting from the neglect of the function F. The tendency of the shock to lie closer to the body as equilibrium is approached is also illustrated. In fact, the equilibrium and exact chemical nonequilibrium shocks nearly coincide downstream. This is not surprising, since, for both analyses, vibrational equilibrium has been assumed, and hence, in the relatively cool region downstream of the nose, similar vibrational levels have been achieved. Moreover, the nonequilibrium species concentrations also will have relaxed more nearly toward the equilibrium values downstream and, in some cases, may even have achieved an over-dissociated level with respect to equilibrium.

The property distributions along the body normals of Fig. 2 are presented in Figs. 3–6. The distance from the

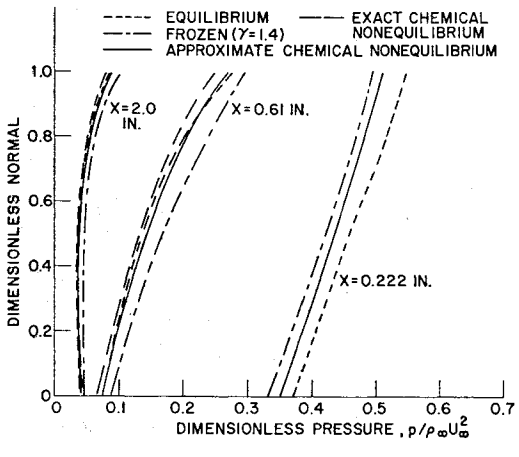

Fig. 3 Pressure along body normals for blunted body of Fig. 2.

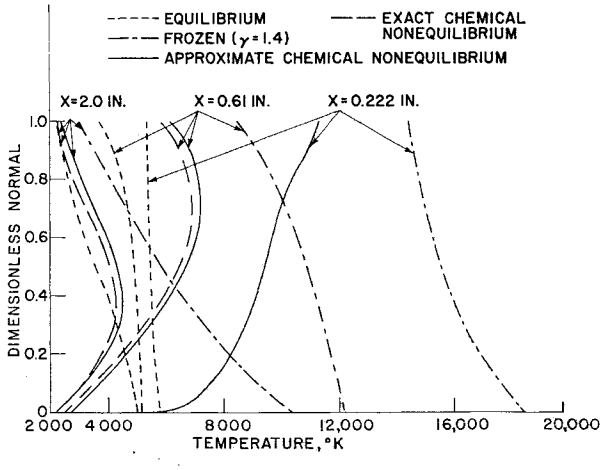

Fig. 4 Temperature along body normals for blunted body of Fig. 2.

body along the normal has been nondimensionalized with respect to the distance to the shock. The approximate and exact nonequilibrium results coincide for the profiles at $x = 0.222$ in., since this is the initial line of the characteristics solutions, as determined from the same blunt-body calculation in both cases. The pressure profiles, nondimensionalized with respect to twice the freestream dynamic pressure, indicate the expected result that pressure differences between equilibrium, frozen, and both approximate and exact chemical nonequilibrium analyses are not great. Thus, even for a blunted body, the neglect of the function F in the Mach line characteristics relations should not cause serious discrepancies in other flow-field variables. The temperature profiles are generally bracketed between the equilibrium and frozen results, with the lower equilibrium values reflecting the greater amount of energy required to reach the equilibrium dissociation level. A rather strong nonequilibrium temperature gradient is observed along the initial line at the body. This is caused by the passage of the body streamline through the stagnation point, where relatively cool near-equilibrium conditions are achieved. The nitric oxide concentration, which is of course zero at the shock, overshoots the equilibrium value and then decreases near the body. The low concentration near the body is attributed to the dissociation of the NO in the expanding downstream flow which follows the original NO formation in the vicinity of the nose. The electron density profiles indicate a general increase in electrons over the equilibrium values across the entire shock layer downstream from the nose, which is due to the higher nonequilibrium initial temperatures immediately behind the shock. The increase is appreciable, particularly over the outer portion of the shock layer. Finally, Figs. 4–6 indicate that only small differences exist between the results of the exact and approximate analyses. This verifies the original assumption that the neglect of the function F and consequent slight variation in the pressure distributions (Fig. 3) would have little effect on the remaining flow-field variables.

A consideration of these profiles in the vicinity of the body indicates a general freezing of the downstream composition. The frozen concentrations will vary across the shock layer, however, with freestream values being achieved at the shock. It should be noted that this freezing does not result in identical downstream profiles, as freezing occurs along streamlines, and a given streamline will cross each profile at a different normal coordinate.

The effects of vibrational relaxation have been determined for the ogival configuration of Fig. 7, traveling at the same velocity and altitude as the blunted body. It is composed of a 40° half-angle conical nose section 0.1 in. in length and a 12° half-angle conical afterbody that is connected to the forecone by a body of revolution intersecting the meridian

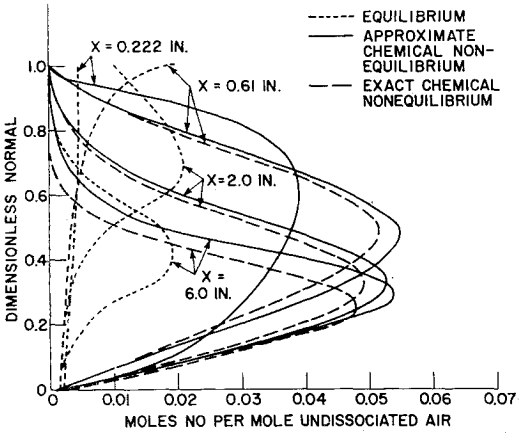

Fig. 5 Nitric-oxide concentration along body normals for blunted body of Fig. 2.

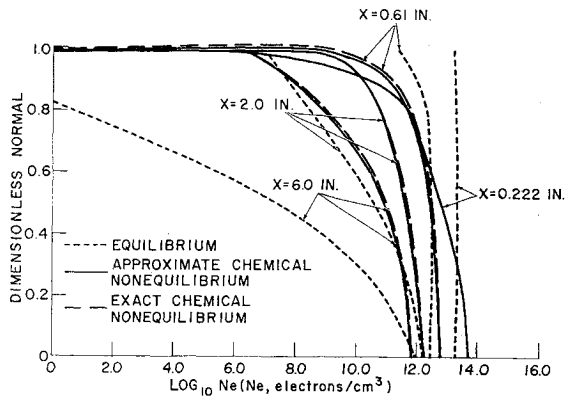

Fig. 6 Electron density along body normals for blunted body of Fig. 2.

plane as a circular arc. Calculations based on the approximate analysis (i.e., neglecting the function F) have been made for chemical relaxation both with and without vibrational equilibrium. The characteristics solution is started at the body normal 0.0766 in. back from the tip. Such a line is sufficiently close to the tip that, for vibrational nonequilibrium, the properties may be determined from a perfect gas conical flow solution, based on the freestream gas constant and specific heat ratio. A similar calculation is made for vibrational equilibrium, except that the gas is now only thermally perfect, with a variable specific heat ratio based on the assumption of the simple harmonic vibrator.

As seen from Fig. 7, the effect of vibrational relaxation on the nonequilibrium shock shape is not great for pointed bodies. (A stronger effect would be exhibited for blunt bodies, however, as may be seen from Ref. 8.) In contrast to the blunt-body results, the nonequilibrium shocks do not tend to coincide with the equilibrium shock downstream; however, this is probably due to the fact that the approximate analysis has been used here (i.e., the behavior is the same as that of the approximate nonequilibrium shock in Fig. 2).

Property distributions along the body normals of Fig. 7 are presented in Figs. 8–10. They exhibit appreciable differences due to vibrational relaxation, with the higher temperature levels resulting in a tendency toward less dissociation and, as seen from Fig. 7, a slight shifting of the shock toward the frozen shape. The electron densities are increased by the inclusion of vibrational relaxation, primarily due to higher initial temperatures immediately behind the shock.

A comparison of the approximate characteristics results with the conventional streamtube technique of Ref. 4 is presented in Figs. 11 and 12 where the property distributions along the body streamline, beginning at the initial profiles of the characteristics solutions, are shown. The assumed pressure distributions for the streamtube analysis were taken from the equilibrium solution for the blunt body and the frozen solution for the ogival body, since these distributions are the closest to reality for these bodies. Good agreement between streamtube and characteristics results is indicated.

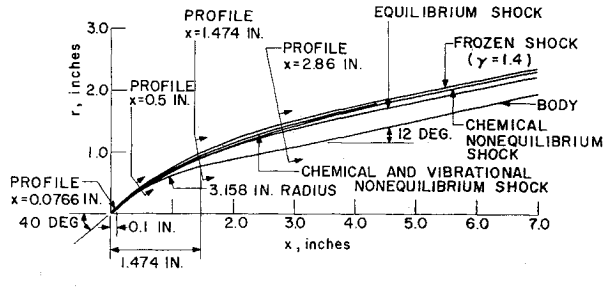

Fig. 7 Geometry for ogival body.

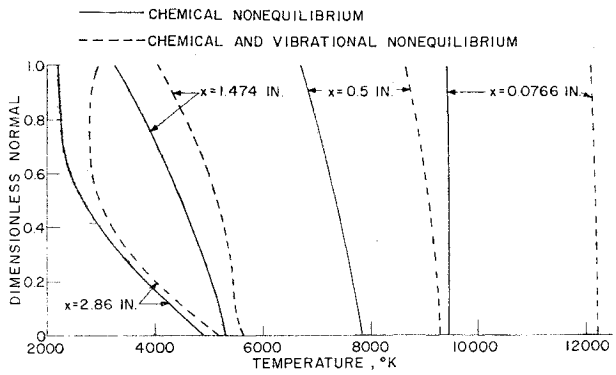

Fig. 8 Temperature along body normals for ogival body of Fig. 7.

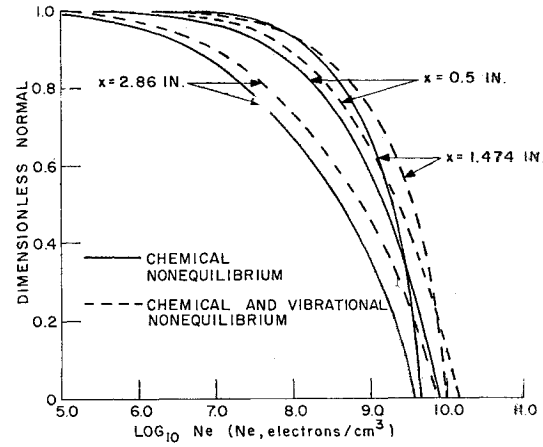

Fig. 10 Electron density along body normals for ogival body of Fig. 7.

There will be a difference in shock shape, however, since the flow-field geometry for the streamtube method is that of the equilibrium or frozen flow used in determining the pressure distribution. The magnitude of this error may be judged from Figs. 2 and 7.

Thus, the streamtube technique can be of use for approximate determination of nonequilibrium flow-field behavior, provided a fine spatial resolution is not required. In this case, only a few streamlines need be used, and a considerable saving in machine time is achieved, as compared to the method of characteristics computation. (The average running time for a single streamline for a body such as that of Fig. 2, for example, is about 1.5 min.) If the resolution is to be comparable with that obtained by a characteristics computation, however, the spacing of the streamlines must be as fine as that of the characteristics grid points, with the result that the total number of nonequilibrium calculations (i.e., the total length of streamlines or streamline characteristic segments) will be of the same order for the two techniques. Since the bulk of the time spent for both analyses is in the nonequilibrium calculations, it is apparent that no saving is achieved by using the streamtube technique in this case, and the more accurate nonequilibrium characteristics computation should be used.

The results of Figs. 11 and 12 also indicate large differences in flow properties on the identical afterbodies of the two configurations due to the variation in nose shape. The differences extend throughout the flow field, as may be seen by comparing the ogival body profiles at $x = 1.474$ in. and 2.86 in. with the blunt-body profiles at $x = 0.61$ in. and 2.0 in., respectively, which are located at identical points in the 12° aftercone. Finally, the relaxation phenomena for both bodies are seen to occur primarily over the nose. The downstream flow is essentially frozen, thus preserving the differences due to nose shape and vibrational relaxation.

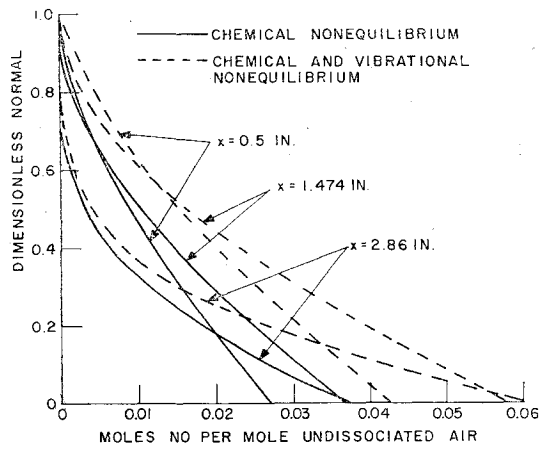

Fig. 9 Nitric-oxide concentration along body normals for ogival body of Fig. 7.

VI. Conclusions

A characteristics technique has been developed for the determination of inviscid nonequilibrium flows. A simplifying approximation has been suggested whereby the function F in the Mach line characteristics relations is neglected. The advantage of such an approximation is not in achieving a reduction in computer program running time (which, indeed, it does not accomplish), but rather to permit a relatively straightforward local combination of a perfect gas characteristics technique with a nonequilibrium streamtube calculation to give a simple approximate nonequilibrium characteristics formulation. Comparison of results from both the exact and approximate formulations under the assumption of vibrational equilibrium has indicated little

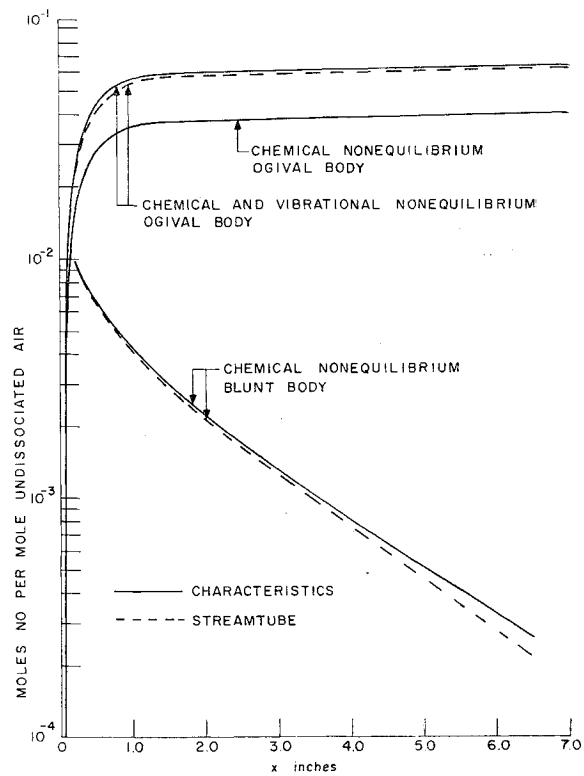

Fig. 11 Nitric-oxide concentration along body streamline.

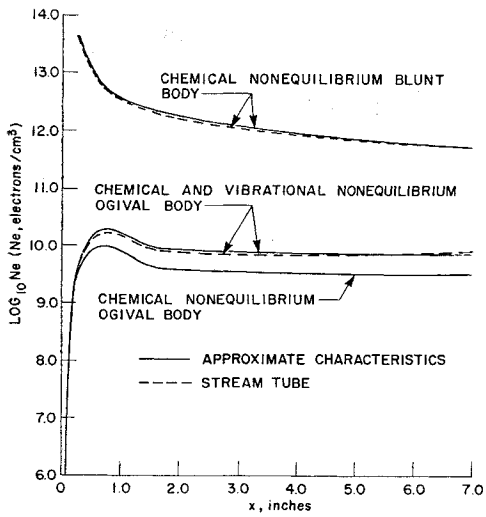

Fig. 12 Electron density along body streamline.

difference in the calculated flow fields, thus justifying the approximation.

The results obtained demonstrate the essential behavior of nonequilibrium flows. Although they become frozen downstream, an upstream nonequilibrium calculation is necessary to determine the frozen composition along each streamline and the point at which it is achieved. The values of the downstream properties exhibit a strong dependence on nose bluntness because of the difference in shock strengths near the nose.

The effects of both chemical and vibrational relaxation are considerable. The results are particularly striking with regard to electron density, where the relaxation processes give rise to electron concentrations higher than the equilibrium values over much of the flow field.

A simple nonequilibrium streamtube analysis, together with a pressure distribution determined from the appropriate equilibrium or frozen calculation, will yield useful approximate results in many cases, particularly if a fine spatial resolution of the flow field is not required. For fine resolution, however, the nonequilibrium characteristics formulation should be used.

Finally, it should be mentioned that only a summary of the problem has been given here. The analysis is presented in more detail, together with additional results, in Ref. 17.

References

[1] Belotserkovskii, O. M., "On the calculation of flow past axisymmetric bodies with detached shock waves using an electronic computing machine," J. Appl. Math. Mech. **24**, 745–755 (1960).

[2] Garabedian, P. R. and Lieberstein, H. M., "On the numerical calculation of detached bow shock waves in hypersonic flow," J. Aeronaut. Sci. **25**, 109–118 (1958).

[3] Ferri, A., "The method of characteristics," *General Theory of High Speed Aerodynamics*, edited by W. R. Sears (Princeton University Press, Princeton, N. J., 1954), Sec. G, p. 583.

[4] Lin, S. C. and Teare, J. D., "A streamtube approximation for calculation of reaction rates in the inviscid flow field of hypersonic objects," *Proceedings of the Sixth Symposium on Ballistic Missile and Aerospace Technology: Reentry* (Academic Press, New York, 1961), Vol. 4, p. 35.

[5] Bloom, M. H. and Steiger, M. H., "Inviscid flow with nonequilibrium molecular dissociation for pressure distributions encountered in hypersonic flight," J. Aerospace Sci. **27**, 821–835 (1960).

[6] Lick, W., "Inviscid flow of a reacting mixture of gases around a blunt body," J. Fluid Mech. **7**, 128–144 (1960).

[7] Hall, J. G., Eschenroeder, A. Q., and Marrone, P. V., "Blunt nosed inviscid air flows with coupled nonequilibrium processes," J. Aerospace Sci. **29**, 1038–1051 (1962).

[8] Springfield, J. F., "Steady, inviscid flow of a relaxing gas about a blunt body with supersonic velocity," *Proceedings of the 1964 Heat Transfer and Fluid Mechanics Institute*, edited by W. H. Giedt and S. Levy (Standford University Press, Standford, Calif., 1964), p. 182.

[9] Capiaux, R. and Washington, M., "Nonequilibrium flow past a wedge," AIAA J. **1**, 650–660 (1963).

[10] Sedney, R., South, J. C., and Gerber, N., "Characteristic calculation of nonequilibrium flows," Aberdeen Proving Ground, Ballistic Research Lab. Rept. 1173 (April 1962).

[11] Sedney, R. and Gerber, N., "Nonequilibrium flow over a cone," AIAA J. **1**, 2482–2486 (1963).

[12] Lee, R. S., "A unified analysis of supersonic nonequilibrium flow over a wedge," IAS Preprint 63-40 (1963).

[13] Brainerd, J. J. and Levinsky, E. S., "Viscous and nonviscous nonequilibrium nozzle flows," AIAA J. **1**, 2474–2481 (1963).

[14] Chu, B. T., "Wave propagation and the method of characteristics in reacting gas mixtures with application to hypersonic flow," Wright Air Development Center TN-57-213, Armed Services Technical Information Agency Doc. AD 118350 (May 1957).

[15] Ferri, A., Libby, P. A., and Zakkay, V., "Theoretical and experimental investigation of supersonic combustion," Aeronautical Research Labs. Rept. ARL 62-467 (September 1962).

[16] Wood, W. W. and Kirkwood, J. G., "Hydrodynamics of a reacting and relaxing fluid," J. Appl. Phys. **28**, 395–398 (1957).

[17] Wood, A. D., Springfield, J. F., and Pallone, A. J., "Determination of the effects of chemical and vibrational relaxation on an inviscid hypersonic flow field," Avco Research and Advanced Development Div. TM-63-88 (January 1964).

[18] Wray, K. L., "Chemical kinetics of high temperature air," *ARS Progress in Astronautics and Rocketry: Hypersonic Flow Research*, edited by F. R. Riddell (Academic Press, New York, 1962), Vol. 7, p. 181–204.

[19] Lin, S. C. and Teare, J. D., "Rate of ionization behind shock waves in air. Part II: Theoretical interpretation," Avco Everett Research Lab., Research Rept. 115 (September 1962).

[20] Eschenroeder, A. Q., Daiber, J. W., Golian, T. C., and Hertzberg, A., "Shock tunnel studies of high-enthalpy ionized airflows," Cornell Aeronautical Lab. Rept. AF-1500-A-1 (July 1962).

[21] Hammerling, P., Teare, J. D., and Kivel, B., "Theory of radiation from luminous shock waves in nitrogen," Phys. Fluids **2**, 422–426 (1959).

[22] Bauer, S. H. and Tsang, S. C., "Mechanisms for vibrational relaxation at high temperatures," Phys. Fluids **6**, 182–189 (1963).

[23] Marrone, P. V. and Treanor, C. E., "Chemical relaxation with preferential dissociation from excited vibrational levels," Phys. Fluids **6**, 1215–1221 (1963).

[24] Heims, S. P., "Moment equations for vibrational relaxation coupled with dissociation," J. Chem. Phys. **38**, 603–606 (1963).

[25] Treanor, C. E. and Marrone, P. V. "Effect of dissociation on the rate of vibrational relaxation," Phys. Fluids **5**, 1022–1026 (1962).

[26] Wray, K. L. and Teare, J. D., "A shock tube study of the kinetics of nitric oxide at high temperatures," J. Chem. Phys. **36**, 2582–2596 (1962).

[27] Hirschfelder, J. O., Curtiss, C. F., and Bird, R. B., *Molecular Theory of Gases and Liquids* (John Wiley and Sons, Inc., New York, 1954), p. 701.